



Lattice thermodynamic behavior in nuclear fuel ThO₂ from first principles

Jianye Liu ^a, Zhenhong Dai ^{a,*}, Xiuxian Yang ^a, Yinchang Zhao ^a, Sheng Meng ^{b, c}

^a Department of Physics, Yantai University, Yantai, 264005, PR China

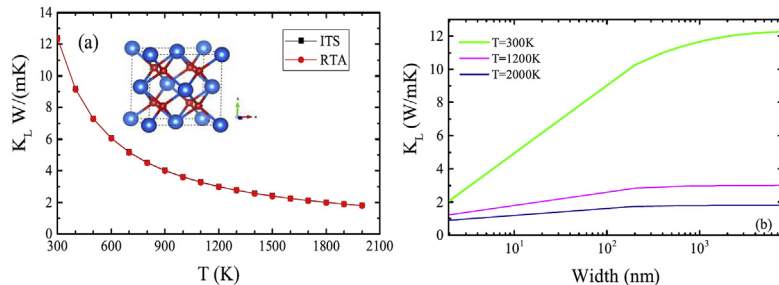
^b Beijing National Laboratory for Condensed Matter Physics and Institute of Physics, Chinese Academy of Sciences, Beijing, 100190, PR China

^c Collaborative Innovation Center of Quantum Matter, Beijing, 100084, PR China

HIGHLIGHTS

- The phase space of three-phonon process of acoustic phonon is large at low frequency, which is different from that of ordinary material.
- The phonon group velocity, relaxation time, Grüneisen parameters and weighted phase space together decided the lattice thermal conductivity.
- We could reasonably design nanostructures of ThO₂ to change the thermal conductivity.

GRAPHICAL ABSTRACT



ARTICLE INFO

Article history:

Received 28 May 2018

Received in revised form

16 August 2018

Accepted 28 August 2018

Available online 1 September 2018

Keywords:

First-principle

Thermodynamic behavior

Acoustic and optical phonon branches

Lattice thermal conductivity

ABSTRACT

Using first-principle calculations and combining with the phonon Boltzmann transport equation, we have systematically investigated the lattice thermodynamic behavior in thorium dioxide (ThO₂) and predicted the lattice thermal conductivity of thorium dioxide from 300 K up to 2000 K. According to the calculated phonon dispersion curves, phonon group velocity, relaxation time, Grüneisen parameters and weighted phase space, the contributions of acoustic and optical phonon branches to the lattice thermal conductivity are estimated. From further analyses, we know that although the phase space of three-phonon process (PW3) of acoustic phonon is large at low frequency, which is different from that of ordinary materials, the valley value appears at 3 THz, resulting in the whole thermal resistance is not too high. So acoustic phonon transports lead to the dominant contributions of the lattice thermal conductivity, while the contributions from optical components is small. Our analyses can make a significance to understand the thermodynamic behaviors of this new type of nuclear fuel dioxide at different temperatures. In addition, by means of the phonon mean-free path and nanowires width, we also studied the size dependence of the lattice thermal conductivity in ThO₂.

© 2018 Elsevier B.V. All rights reserved.

1. Introduction

With the ever-growing world energy requirements, the research on the development of new energy sources or the improvement of energy conversion efficiency have received increasing attentions. So far we still get a lot of energy through

* Corresponding author.

E-mail addresses: zhidai@ytu.edu.cn (Z. Dai), y.zhao@ytu.edu.cn (Y. Zhao), smeng@iphy.ac.cn (S. Meng).

the fissile nuclear reactor, in which uranium dioxide (UO₂) is one of the most common nuclear-fission fuel components [1–5]. However, its low lattice thermal conductivity at high temperatures directly influences its thermal stability and working temperature [6,7]. Moreover, in the uranium dioxide nuclear reaction, a large amount of rare earth elements are generated in the radioactive waste [8]. And these radioactive wastes are highly radioactive and difficult to handle. Therefore, a number of experiments and effects in recent years have been done to search possible alternatives to (UO₂). Among thorium based compounds, thorium dioxide (ThO₂), which produces less transuranic (TRU) than uranium-based fuels, is considered a good candidate to uranium dioxide in fissile nuclear reactors. In addition, thorium based fuels which is almost entirely considered fertile in nature can efficiently reduce plutonium stockpiles by using a mixed oxide fuel (MOX) of thorium and plutonium in the nuclear reactor while maintaining acceptable safety and control characteristics of the reactor system [9]. Compared with the uranium dioxide fuels, One attraction of using the thorium dioxide in fissile nuclear reactors is due to its relatively improved thermo-physical properties, such as higher melting points, higher thermal conductivity and lower coefficient of thermal expansion [10]. In recent years, the performance of thorium-based fuels in fissile nuclear reactors has been tested and studied from many research groups [11,12].

In fact, metal thorium and its compounds has been extensively investigated ever since 1950. In the early stage, people conducted a series of experimental measurements of the thermal expansion coefficient, heat capacity and thermal conductivity of ThO₂ [13–17]. For instance, the valence-band structures of the thorium and its dioxides have been investigated by means of x-ray photoemission spectroscopy by Veal et al. [18] in 1974. In addition, the thermal properties of ThO₂ were seriously assessed by means of comparing with the measured values by Bakker et al. [19] in 1997. Besides, we can also obtain the thermal properties of ThO₂ from a thermal-physical database of materials for light water reactors and heavy water reactors which was established by the International Atomic Energy Agency (IAEA) [20]. Later, many groups separately carried out the work on the mechanical properties and electronic structures, ground-state properties and phase transition at high pressure, elastic and optical properties of thorium dioxide [21–26].

Although previous investigators have done so much research, it is essential to systematically study the phonon thermal transport in thorium dioxide, which is crucial for its application in the fissile nuclear reactor. Thus, in our work, with the help of calculated phonon dispersion curves, phonon group velocity, relaxation time at different temperature, Grüneisen parameters and weighted phase space, we comprehensively discuss the contributions of acoustic and optical phonon branches to the lattice thermal conductivity for thorium dioxide. The rest of this paper is organized as follows. In Sec. 2, we roughly presented the theoretical calculation methods. In Sec. 3, the computing results of the thermal conductivity and the discussion of the phonon thermal transport are appeared. Finally, we give our summary in Sec. 4.

2. Methodology

To get accurate thermal transport consequences, all the calculations are carried out by employing the Vienna ab-initio simulation package (VASP) on the basis of the first-principles density functional theory (DFT) [27,28]. By means of the phonon Boltzmann transport equation (BTE), we can obtain the lattice thermal conductivity. Then the κ_L along the α direction can be written as

$$\kappa_L^{\alpha\alpha} = \frac{1}{k_B T^2 \Omega N} \sum_{\mathbf{k}, \lambda} f_0 (f_0 + 1) (\hbar \omega_{\mathbf{k}, \lambda}) v_g^{\alpha, \mathbf{k}, \lambda} F_{\mathbf{k}, \lambda}^{\alpha} \quad (1)$$

where k_B , T , Ω and N are the Boltzmann constant, the thermodynamic temperature, the unit cell volume and the number of q points in the first Brillouin zone (BZ), respectively. Afterwards \mathbf{k} is wave vector, λ is phonon branch and f_0 is the equilibrium Bose-Einstein distribution function. \hbar is the reduced Planck constant, $\omega_{\mathbf{k}, \lambda}$ express the phonon frequency at phonon mode λ , and $v_g^{\alpha, \mathbf{k}, \lambda}$ is the phonon group velocity of at phonon mode λ along the α direction. The last element $F_{\mathbf{k}, \lambda}^{\alpha}$ in Eq. (1) is defined as the formula [29].

$$F_{\mathbf{k}, \lambda}^{\alpha} = \tau_{\mathbf{k}, \lambda} (v_g^{\alpha, \mathbf{k}, \lambda} + \Delta_{\mathbf{k}, \lambda}) \quad (2)$$

where $\tau_{\mathbf{k}, \lambda}$ is the phonon lifetime in relaxation time approximation (RTA). $\Delta_{\mathbf{k}, \lambda}$ is a correction term used to eliminate the inaccuracy of RTA via solving the BTE iteratively. If $\Delta_{\mathbf{k}, \lambda}$ is equal to zero, the $\kappa_L^{\alpha\alpha}$ in RTA is obtained.

The lattice thermal conductivity κ_L of thorium dioxide are calculated by the ShengBTE code [29]. The interatomic force constants (IFCs) which divide into harmonic and anharmonic are acquired within the $3 \times 3 \times 3$ supercells by finite-difference approach, which are computed based on the density functional theory (DFT) software package VASP, by means of the PHONOPY program [30] and the THIRDORDER.PY script [29], respectively. In DFT calculations, we selected the generalized gradient approximation (GGA) of the Perdew-Burke-Ernzerhof (PBE) parametrization for the exchange-correlation functional [31]. In addition, the projector-augmented-wave potentials (PAW) [32] is used to describe as the ion core, and a plane-wave basis set is confined to the cutoff energy of 520 eV. A $9 \times 9 \times 9$ Γ -centered Monkhorst-Pack k -mesh is used to simulate during structural relaxation of primitive cell until the energy differences are converged within 10^{-8} eV, with a Hellman-Feynman force convergence threshold of 10^{-4} eV/Å. Then, for the calculations of phonon dispersion, The $3 \times 3 \times 3$ supercell with $3 \times 3 \times 3$ k -mesh is used to ensure the convergence. Finally, The $3 \times 3 \times 3$ supercell are used to get the anharmonic (IFCs), and the interaction up to the third nearest neighbors is included. For the ShengBTE calculations, The same $3 \times 3 \times 3$ supercell with a $27 \times 27 \times 27$ q -mesh are used to simulate the corresponding q space integration.

3. Results and discussion

Previous research have shown that the thorium 5f states become delocalized after electronic hybridizations, so adding additional U and J modifications probably result in the incorrect results [9,24,33]. So DFT calculations with the generalized gradient approximation (GGA) of the Perdew-Burke-Ernzerhof (PBE) parametrization for the exchange-correlation functional are appropriate enough for gaining the phonon transport properties of ThO₂.

The optimized structure of ThO₂ is shown in Fig. 1. Fig. 1(a) is the primitive cell and Fig. 1(b) is the corresponding conventional cell of ThO₂. Thorium dioxide is crystallized in a CaF₂-like ionic structure and the conventional cell for ThO₂ belongs to space group Fm $\bar{3}$ m. Its primitive cell consists of one Th atom and two O atoms while the conventional cell is made up of four ThO₂ formula units with four thorium atoms and eight oxygen atoms, respectively. Each O atom is connected to the surrounding suitable Th atoms to form a tetrahedron structure. A feature of this structure is the presence of a large octahedral space [24]. In this work, our optimized lattice parameter a_0 is 5.61 Å, which is in good accordance with the previous experimental data of 5.60 Å [34,35].

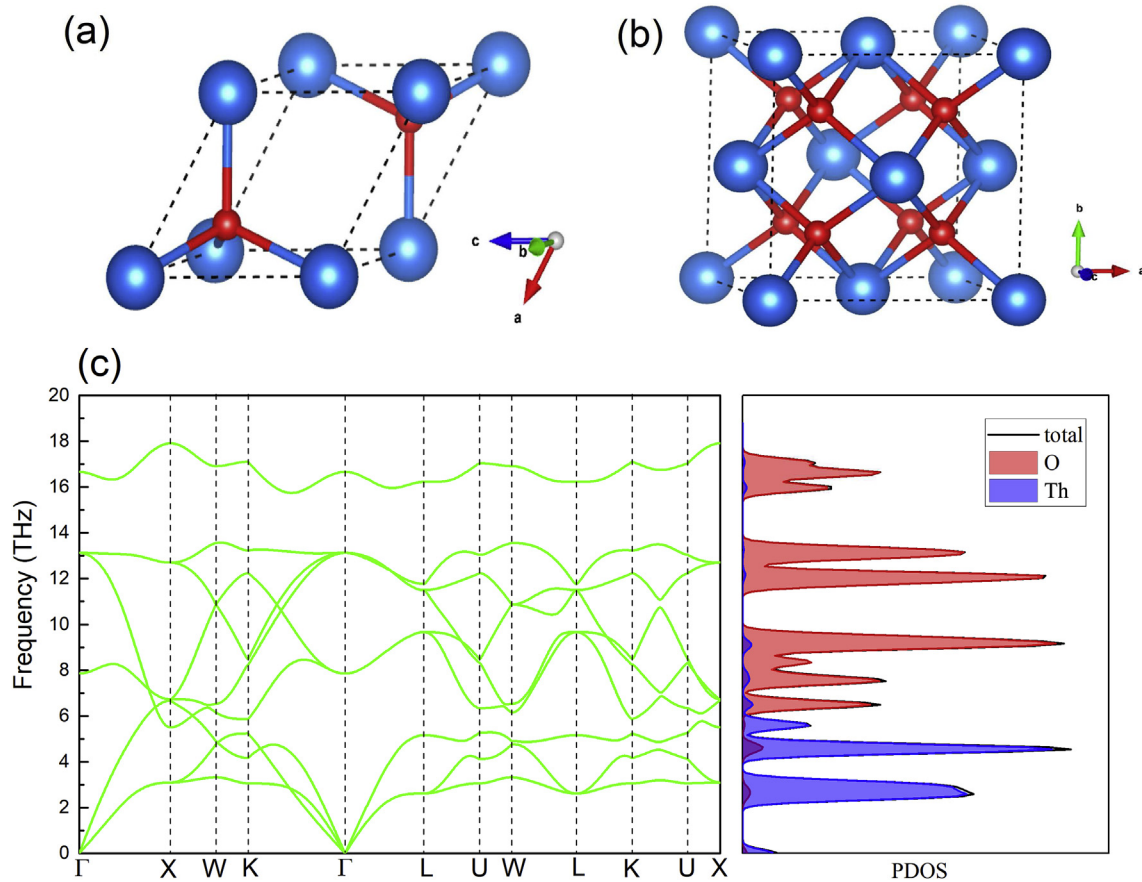


Fig. 1. (Color online). Crystal structure of the pristine ThO_2 . (a) the primitive unit cell; (b) the conventional unit cell. The blue and red balls represent the Th and O atoms, respectively; (c) Phonon dispersion and phonon density of states (PDOS) of ThO_2 , the acoustic (optical) branches arise almost completely from the vibrations of thorium atoms (oxygen atoms). (For interpretation of the references to colour in this figure legend, the reader is referred to the Web version of this article.)

The phonon dispersion curves are one of the basic aspects for investigating the phonon transport. Hence, we calculated the phonon dispersion spectrum along the high-symmetry k -point lines in the Brillouin zone along with the phonon density of states (PDOS), which are plotted in Fig. 1(c). Because there are only three atoms for ThO_2 in each primitive cell, 9 phonon branches exist in the dispersion curves. There are two transverse acoustic (TA) modes and one longitudinal acoustic (LA) mode, as well as four transverse optical (TO) modes and two longitudinal optical (LO) modes, respectively. As shown in the figure, there is almost no obvious gap between the acoustic and the optical branches, while an overlap between longitudinal acoustic (LA) and transverse optical (TO) modes around the X point has clearly presented. Furthermore, we calculated the Born effective charge and the dielectric constants by DFPT in VASP and obtained an accurate splittings of longitudinal (LO) and transverse optical (TO) modes [36]. For ThO_2 , the Born effective charges of the thorium atom and the oxygen atom are $5.40 e$ and $-2.70 e$, respectively, together with the dielectric constant ϵ being 4.80, which are both consistent with that in Ref. [9]. As we expected, the optical branches have evident splitting of TO and LO modes at the Γ point. On the other hand, the partial PDOS tell us that at low frequency (0–6 THz) the vibrations of thorium atom are governed mainly while oxygen atom dominates the vibrations at high-frequency (6–18 THz), which is owing to the heavier mass of thorium atom than that of oxygen atom.

The calculated lattice thermal conductivity κ_L of the naturally occurring ThO_2 is plotted in Fig. 2. One can see that with the rising of temperature, the lattice thermal conductivity has reduced

continuously from 300 K to 2000 K in Fig. 2(a), which is in accordance with most of the situation. For ThO_2 , the values of κ_L are 12.40 W/mK, 3.01 W/mK and 1.81 W/mK at 300 K, 1200 K and 2000 K respectively which is in good agreement with previous work [9,15–17,19]. In addition, by comparing the results with uranium dioxide [6,37,38], we find that the κ_L is slightly larger than that of UO_2 at high temperature. Furthermore, the RTA results and iterative solutions (ITS) of the BTE are both exhibited, which are wonderfully consistent with each other. And iterative solutions (ITS) are obtained by repeated calculations, in which the distribution function of each calculation of Boltzmann transport equation serves as the initial value of the next iteration calculation until to the final convergence results. Then in Fig. 2(b), the ratio between the cumulative thermal conductivity and lattice thermal conductivity as a function of the phonon frequency have been shown at 300 K, 1200 K and 2000 K, respectively. On the one hand, these curves specify a cutoff angular frequency when calculating the contribution of different phonon modes. We can indicate that the κ_L of ThO_2 is 70% dominated by the phonons with the frequency below 6 THz, which all lie in the range of the acoustic phonon modes. And the rest of 30% is dedicated between 6 THz and 12 THz, which is contributed by the optical phonon branches. On the other hand, the trend of the contribution of different phonon modes is almost independent of the change of temperature.

In order to evaluate the contribution of different phonon branches to lattice thermal conductivity, we first calculate the phonon group velocities of different phonon branch modes. The phonon group velocities of all phonon modes within the first

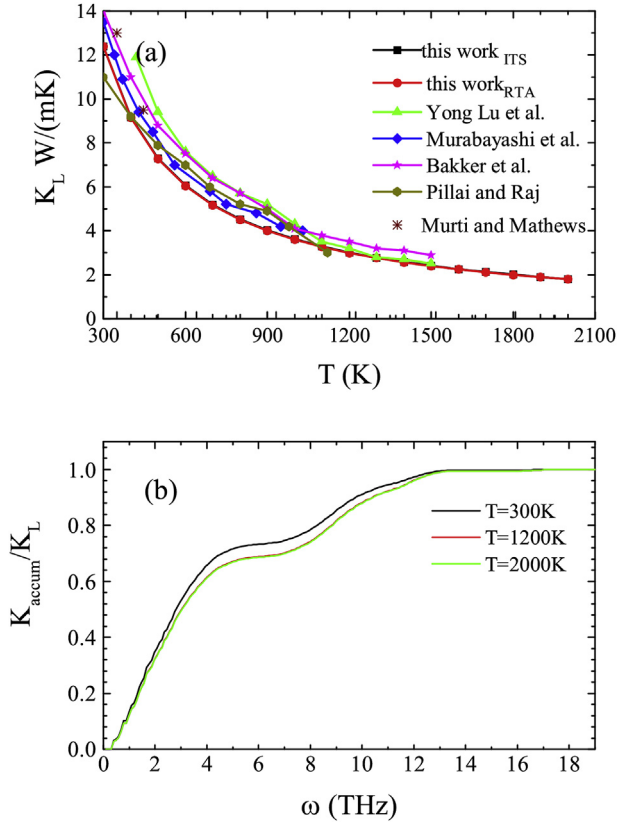


Fig. 2. (Color online). (a) Calculated lattice thermal conductivity κ_L of naturally occurring ThO_2 as a function of temperature T ranging from 300 K to 2000 K. The black square and red circle lines represent our ITS (RTA) results for ThO_2 . Theoretical results from Yong Lu et al. [9] and experiment results from Murabayashi et al. [15], Pillai and Raj [16], Murti and Mathews [17] and Bakker et al. [19] are displayed for comparison. (b) The scaled cumulative thermal conductivity versus the allowed phonon frequency at 300 K, 1200 K and 2000 K, respectively. (For interpretation of the references to colour in this figure legend, the reader is referred to the Web version of this article.)

Brillouin zone (BZ) as a function of frequency are shown in Fig. 3. The phonon group velocity is determined by

$$v_g = \frac{d\omega_\lambda}{d\mathbf{k}} \quad (3)$$

where v_g is phonon group velocities, ω_λ is phonon frequency of λ th phonon branch and \mathbf{k} is wave vector. In Fig. 3, the red, green and blue pattern represent the TA_1 , TA_2 , LA modes, respectively and the orange, violet, dark yellow, wine, dark cyan and gray signify TO_1 ,

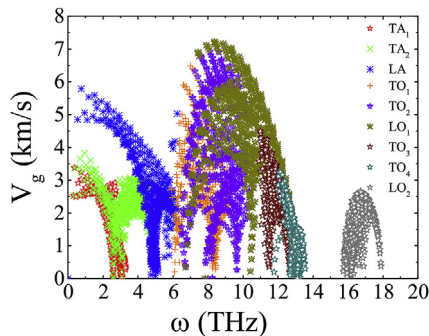


Fig. 3. (Color online). Phonon group velocities of all phonon modes within the first Brillouin zone as a function of frequency for ThO_2 .

TO_2 , LO_1 , TO_3 , TO_4 and LO_2 phonon branches, separately. For ThO_2 , the maximum group velocities are about 3.37 km/s, 3.82 km/s, 5.79 km/s, 6.49 km/s, 6.93 km/s, 7.23 km/s, 4.49 km/s, 3.25 km/s and 2.66 km/s for TA_1 , TA_2 , LA, TO_1 , TO_2 , LO_1 , TO_3 , TO_4 and LO_2 phonon branches, respectively. One can see that the phonon group velocity of LA mode is bigger than that of the other acoustic phonon modes in Fig. 3. And the phonon group velocity of LO_1 mode is the maximum in all phonon modes. According to the Eq. (1), the original κ_L is $\propto v_g$, which means that if other conditions remain constant, the higher the group velocities of phonon modes, the bigger the contribution to the thermal conductivity. We can indicate that the acoustic and optical phonon modes below the frequency of 12.2 THz and above the phonon group velocities of 3.25 km/s play a significant role for the κ_L , which is corresponding to the results of Fig. 2(b). Further, combining with Figs. 2(b) and Fig. 3, we can infer that the acoustic phonon modes have dominant contribution to lattice thermal conductivity.

In order to further explore the factors affecting thermal conductivity, we obtain specific heat of the crystal as a function of temperature ranging from 300 K to 2000 K and the calculated Grüneisen parameters as a function of frequency for ThO_2 within the first BZ in Fig. 4. The unit volume heat capacity is the sum of all phonon modes within the Brillouin zone (BZ),

$$C_v(T) = \sum_{\lambda, \mathbf{k}} C_{v, \mathbf{k}}(\mathbf{k}, T) \quad (4)$$

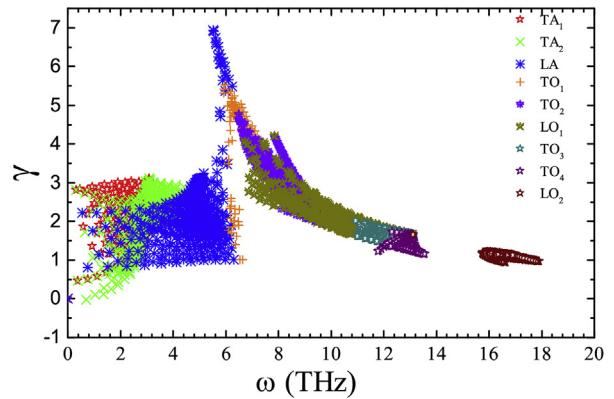
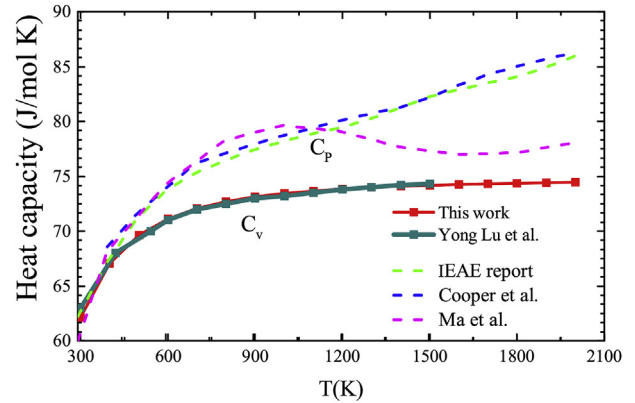


Fig. 4. (Color online). (a) Specific heat of the system as a function of temperature ranging from 300 K to 2000 K. The solid line and dotted line represent heat capacities at constant volume (C_v) and constant pressure (C_p), respectively. Experiment data from IEAE report [20] and modelling data from Yong Lu et al. [9], Ma et al. [39], Cooper et al. [40] are exhibited for comparison. (b) The calculated Grüneisen parameters of each phonon branch as a function of frequency for ThO_2 within the first BZ.

where $C_v(T)$ is the total specific heat of the crystal, \mathbf{k} is wave vector, $C_{v,\mathbf{k}}$ is the phonon mode contribution to the specific heat and given by

$$C_{v,\mathbf{k}}(\mathbf{k}, T) = k_B \sum_{\lambda, \mathbf{k}} \left(\frac{\hbar \omega_{\lambda}(\mathbf{k}, V)}{2k_B T} \right)^2 \frac{1}{\sinh^2[\hbar \omega_{\lambda}(\mathbf{k}, V)/2k_B T]} \quad (5)$$

where κ_B is Boltzmann constant, $\omega_{\lambda}(\mathbf{k}, V)$ is the phonon frequency of the λ th phonon mode. Then the relationship between κ_L and specific heat capacity can be expressed in the following terms [41].

$$\kappa_L = \frac{1}{3} C_v \tau \bar{v}^2 \quad (6)$$

where τ is the relaxation time, the \bar{v} is the average phonon group velocity. As shown in Fig. 4(a), with the rising of temperature, the specific heat capacity at constant volume increases continuously until it finally tends to be smooth. One can see that the maximal value of C_v approaches to 74 J/molK which is in good agreement with the previous work from 300 K to 1500 K [9]. In addition, we also show the specific heat capacity at constant pressure (C_p) as a function of temperature by citing relevant literature [20,39,40]. Afterwards, the mode (γ_j) Grüneisen parameter often provides the anharmonic interactions information, and is defined by

$$\gamma_j(\vec{k}) = -\frac{a_0}{\omega_{\lambda}(\vec{k})} \frac{\partial \omega_{\lambda}}{\partial a} \quad (7)$$

where γ_j is the Grüneisen parameter, \vec{k} is the wave vector, a_0 is the equilibrium lattice constant, λ is phonon branch index, and $\omega_{\lambda}(\vec{k})$ is the frequency of λ th phonon branch. One can see that the γ_j of all phonon modes are both greater than zero in Fig. 4(b) which

indicates that these phonon modes must consider the anharmonic approximation and hence almost all of them have effects on κ_L . We can know that the stronger the anharmonic interactions is, the more intense the phonon scattering is, and the lower the contribution to thermal conductivity is. Therefore, the TA_1 , TA_2 and the great mass of LA modes are dominant to the lattice thermal conductivity due to their weaker phonon scattering and relatively higher group velocities. In short, the phonon group velocities and the Grüneisen parameter are fundamental to discuss the phonon transport in ThO_2 .

In order to investigate the detailed phonon thermal transport mechanism, it is worthwhile to study the relaxation times of each phonon mode as a function of frequency. Because the length of phonon relaxation times reveal the strength of anharmonic interactions, the stronger the anharmonic interactions, the shorter the phonon relaxation times are. In addition, according to the Eq. (1), the τ can impact the thermal conductivity, thus we studied the relaxation times of ThO_2 . As shown in Fig. 5, we calculate the isotopic, anharmonic and total relaxation times as a function of frequency at 300 K, 1200 K and 2000 K, respectively. In SHENGBTE calculations, as a result of the elimination of boundary scattering effect, the inverse of total relaxation time is obtained by anharmonic three-phonon scattering and isotopic scattering [42–45] through the formula of

$$\frac{1}{\tau_{\lambda}(\vec{k})} = \frac{1}{\tau_{\lambda}(\vec{k})^{anh}} + \frac{1}{\tau_{\lambda}(\vec{k})^{iso}} \quad (8)$$

where the $\frac{1}{\tau}$ is the scattering rates. First we obtain the isotopic relaxation time, as shown in Fig. 5(a), (d) and (g). One we can see

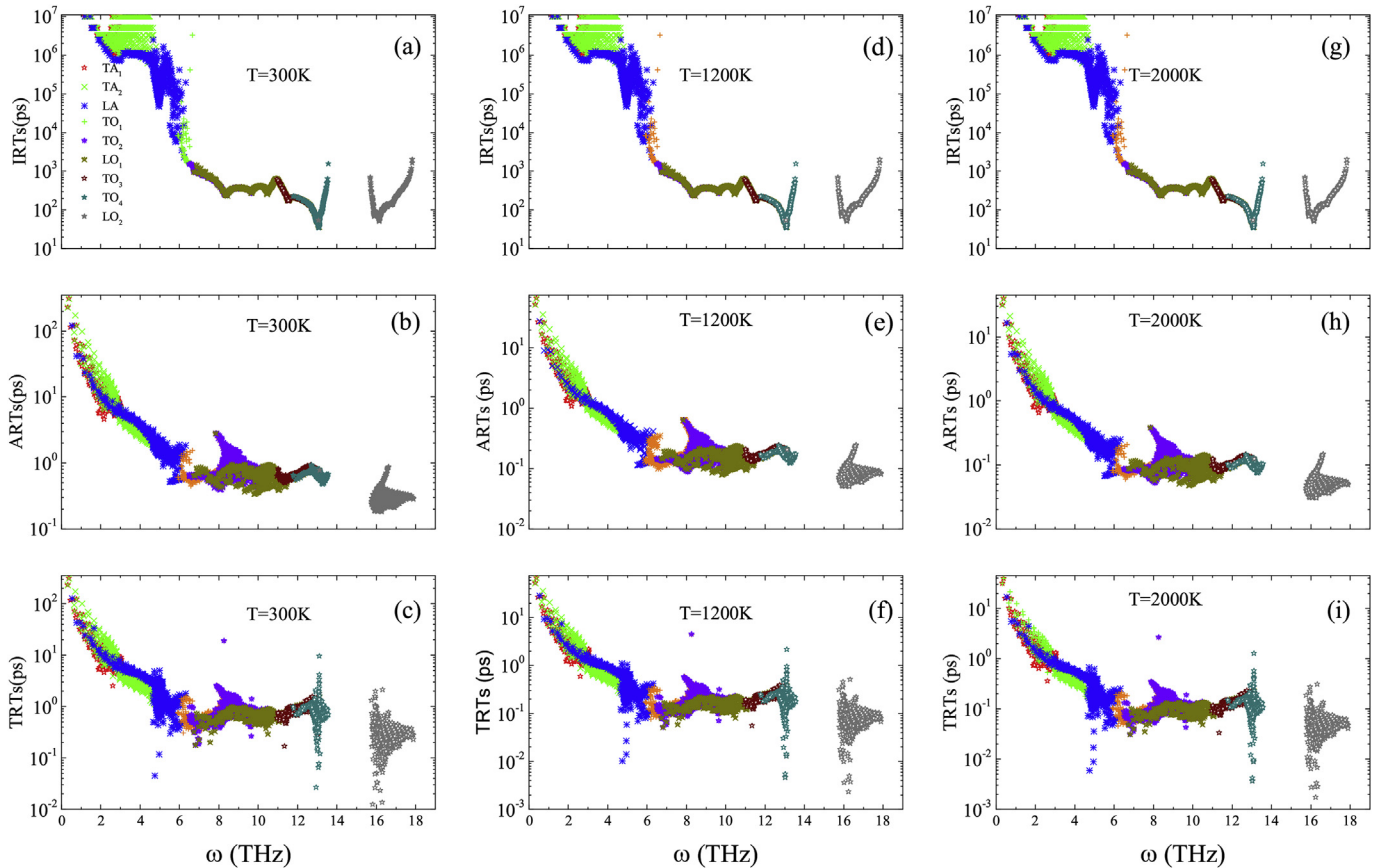


Fig. 5. (Color online). The isotopic (a), (d), (g) anharmonic (b), (e), (h) and total relaxation time (c), (f), (i) of each phonon branch as a function of frequency at 300 K, 1200 K and 2000 K, respectively.

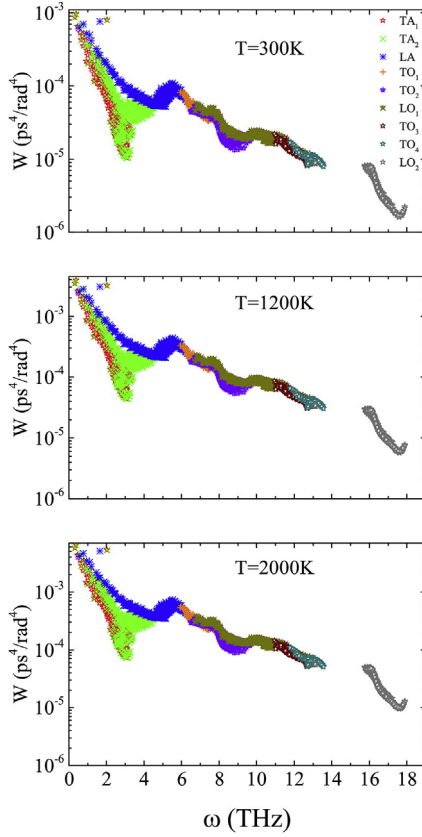


Fig. 6. (Color online). The corresponding weighted phase space WP3 of different phonon modes at 300 K, 1200 K and 2000 K, respectively.

that isotopic scattering processes are temperature-independent and frequency-dependent. The phonons of long-wavelength can transmit nearly all the heat with very weak isotopic scattering [46], hence we have observed the relative long isotopic relaxation time for acoustic phonon modes at low frequencies. However, the isotopic scattering process is weak while the anharmonic scattering process which corresponds to three-phonon process is strong by comparing with Fig. 5(b), (e), (h) and Fig. 5(c), (f), (i). Because the phonon branches with the longer relaxation time will dominate the lattice thermal conductivity, then in Fig. 5(c), (f), (i), the acoustic phonon TA₁, TA₂ and LA modes which have larger values of total relaxation time than other optical modes make a major contribution to lattice thermal conductivity. In addition, we can also observe that with the increase of temperature, the value of relaxation time has reduced while the trend has not changed too much on the whole from Fig. 5(b), (e), (h) and Fig. 5(c), (f), (i). And the reduction of relaxation time with the increase of temperature just proves that the enhanced three-phonon processes reduce thermal conductivity.

As we all know, the $\tau_{\lambda}(k)^{anh}$ is gained by the sum of the three-phonon transition probabilities $\Gamma_{\lambda\lambda'\lambda''}^{\pm}$, which can be expressed as

$$\Gamma_{\lambda\lambda'\lambda''}^{+} = \frac{\hbar\pi}{4} \frac{f'_{\lambda} - f''_{\lambda}}{\omega_{\lambda}\omega_{\lambda'}\omega_{\lambda''}} \left| V_{\lambda\lambda'\lambda''}^{+} \right|^2 \delta(\omega_{\lambda} + \omega_{\lambda'} - \omega_{\lambda''}) \quad (9)$$

$$\Gamma_{\lambda\lambda'\lambda''}^{-} = \frac{\hbar\pi}{4} \frac{f'_{\lambda} + f''_{\lambda} + 1}{\omega_{\lambda}\omega_{\lambda'}\omega_{\lambda''}} \left| V_{\lambda\lambda'\lambda''}^{-} \right|^2 \delta(\omega_{\lambda} - \omega_{\lambda'} - \omega_{\lambda''}) \quad (10)$$

where f'_{λ} represents $f_{\lambda}(\omega_{\lambda})$ and so forth for simplicity. On the one hand, $\Gamma_{\lambda\lambda'\lambda''}^{+}$ is corresponding to absorption processes, which

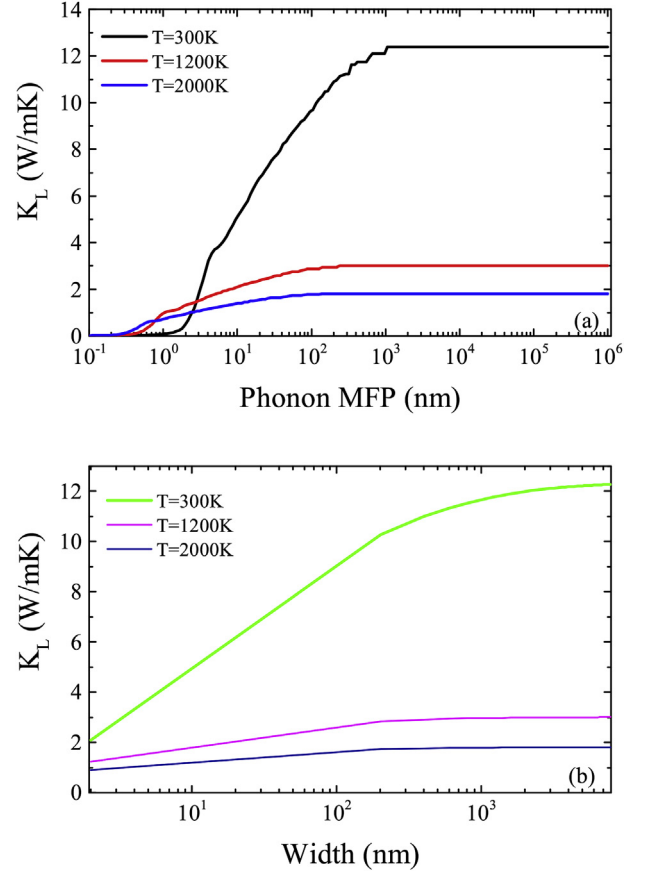


Fig. 7. (Color online). Cumulative lattice thermal conductivity κ_L of ThO₂ with respect to the phonon MFP (a) and thermal conductivities of ThO₂ nanowires along [100] direction as a function of width (b) at 300 K, 1200 K and 2000 K, respectively.

is resulting in only one phonon with the combined energy of two incident phonons. On the other hand, $\Gamma_{\lambda\lambda'\lambda''}^{-}$ stands for emission processes in which the energy of one $\lambda\lambda'\lambda''$ incident phonon is split into two phonons [29]. $\Gamma_{\lambda\lambda'\lambda''}^{\pm}$ depends on the anharmonic IFC3 and the weighted phase space of three-phonon process (WP3) [47,48]. The intensity of IFC3 which corresponds to the anharmonic property of phonon modes is usually characterized by the Gruneisen parameter. In addition, we provide WP3 to estimate the number of scattering channels for each phonon mode due to the fact that WP3 dominates a great deal of scattering events of conforming to the energy and momentum conservation conditions [44,49]. One can deduce that the three-phonon processes in phase space are unlimited when there are a large number of available scattering channels. Thus, the WP3 is a forceful criterion of the κ_L as previous research have shown [50]. To obtain further study on the mechanism of the phonon scattering, we calculated the WP3 as a function of frequency which are shown in Fig. 6. But we obtain an anomalous behavior that the WP3 of acoustic phonon modes are bigger than that of optical modes in the low frequency and then arrive at the lowest values at about 3 THz. At low frequency, most of the acoustic phonon are concentrated at the center of the Brillouin zone Γ point, the Umklapp processes are rare, so the resistance from the three phonon scattering is small, especially, when the phonon frequency increase to 3 THz, the scattering channels became very small, all these means that the acoustic phonon modes have less effective scattering rates and more contributions to the phonon thermal transport. Moreover, we can also see that with the increase of temperature,

the value of WP3 has raised while the trend has not changed too much on the whole.

As is well known, we can improve the contribution of the edge states by optimizing geometric dimensions to reduce the thermal resistance and achieve better thermoelectric performance [44]. Thus, as shown in Fig. 7(a), we examine the size dependence of κ_L by calculating the cumulative thermal conductivity as a function of mean free path (MFP) at 300 K, 1200 K and 2000 K, respectively. One can see that the κ_L keeps increasing with the value of MFP rising continually, eventually getting to the thermodynamic limit above a length L_{diff} in Fig. 7(a). The L_{diff} which represents the longest mean free path of thermal medium [51,52] is 1059.50 nm, 240.94 nm and 138.26 nm at 300 K, 1200 K and 2000 K, respectively. Furthermore, we calculate that phonons with MFPs below 79.34 nm, 15.00 nm and 8.6 nm devote about 75% of the total κ_L at 300 K, 1200 K and 2000 K, respectively. This signifies that we can change thermal conductivity properly by increasing or decreasing the characteristic length of nanostructures. Then when we investigate a nanowire system, phonons long MFPs will be dispersed by the strongly boundary scattering which results in the confined contribution to κ_L . In other words, due to grain boundary effects, the stronger the boundary scattering, the lower the contribution to thermal conductivity. As shown in Fig. 7(b), we obtain the thermal conductivity of the ThO₂ nanowires as a function of the width at 300 K, 1200 K and 2000 K, respectively. One can also observe that as the width broadens, the κ_L keeps increasing continuously until reaching the maximum. All the maximum of the κ_L corresponds to the nanowire width of 7.60 μm at different temperature. In addition, a nanowire with the width of 202 nm contribute 83.6%, 94.7% and 96.7% to the total κ_L at 300 K, 1200 K and 2000 K, respectively. Finally, we can both observe that the slope of a curve keep falling with the increase of temperature in Fig. 7(a) and (b) which implies the effect of nanowire width and MFP on thermal conductivity is reduced with the increase of temperature.

4. Conclusion

In summary, we calculate the lattice thermal conductivity κ_L and investigate thoroughly the phonon thermal transport of ThO₂ by combining the phonon Boltzmann transport theory together with the first-principles calculations. The lattice thermal conductivity has decreased with the raise of temperature from 300 K to 2000 K. Further analyses reveal that the acoustic phonon modes which is below 6 THz contribute about 70% to κ_L , while the optical modes contribute the rest of κ_L . By means of the investigation of phonon thermal transport, we find that the acoustic phonon modes possess a relatively big weighted phase space WP3 in low frequency but a comparatively long anharmonic relaxation times (ARTs) which means the weak resistance from the effective three-phonon scattering process. At the same time, acoustic phonon modes have relatively high phonon group velocity and the relatively low Grüneisen parameter, which lead to high lattice thermal conductivity κ_L . We can conclude that the acoustic phonon branches dominate the lattice thermal conductivity. In addition, based on the relationship between the κ_L and the mean free path (MFP) together with nanowires width, we could reasonably design nanostructures of ThO₂ to change the thermal conductivity.

Acknowledgment

This research were supported by the National Key Research and

Development Program of China under Grant No.2016YFA0300902, the National Natural Science Foundation of China under Grant No.11774396 and No.11704322, Shandong Natural Science Funds for Doctoral Program under Grant No.ZR2017BA017.

References

- [1] Belle, J. Nucl. Mater. 30 (1969) 3.
- [2] J. Killeen, J. Nucl. Mater. 88 (1980) 185.
- [3] K.N. Kudin, G.E. Scuseria, R.L. Martin, Phys. Rev. Lett. 89 (2002) 266402.
- [4] B. Dorado, B. Amadon, M. Freyss, M. Bertolus, Phys. Rev. B 79 (2009) 235125.
- [5] B. Dorado, G. Jomard, M. Freyss, M. Bertolus, Phys. Rev. B 82 (2010) 035114.
- [6] J. Fink, J. Nucl. Mater. 279 (2000) 1.
- [7] V.V. Rondinella, T. Wiss, Mater. Today 13 (2010) 24.
- [8] L. Petit, A. Svane, Z. Szotek, W.M. Temmerman, G.M. Stocks, Phys. Rev. B 81 (2010) 045108.
- [9] Y. Lu, Y. Yang, P. Zhang, J. Phys. Condens. Matter 24 (2012) 225801.
- [10] M.W.D. Cooper, C.R. Stanek, X.-Y. Liu, D.A. Andersson, MRS Advances 1 (2016) 2483.
- [11] J. Herring, P.E. MacDonald, K.D. Weaver, C. Kullberg, Nucl. Eng. Des. 203 (2001) 65.
- [12] A. Nez-Carrera, J.L.F. Lacouture, C.M. del Campo, G. Espinosa-Paredes, Energy Convers. Manag. 49 (2008) 47.
- [13] J.P. Moore, T.G. Kollie, R.S. Graves, D.L. McElroy, Tech.Rept.Oak Ridge National Laboratory Report ORNL-4121, 44, 1967.
- [14] A. Momin, M. Karkhanavala, High Temp. Sci. 10 (45) (1978).
- [15] M. MURABAYASHI, J. Nucl. Sci. Technol. 7 (1970) 559. <https://www.tandfonline.com/doi/pdf/10.1080/18811248.1970.9734742>.
- [16] C. Pillai, P. Raj, J. Nucl. Mater. 277 (2000) 116.
- [17] P.S. Murti, C.K. Mathews, J. Phys. Appl. Phys. 24 (1991) 2202.
- [18] B.W. Veal, D.J. Lam, Phys. Rev. B 10 (1974) 4902.
- [19] K. Bakker, E. Cordfunke, R. Konings, R. Schram, J. Nucl. Mater. 250 (1997) 1.
- [20] I.A.E. Agency, Thermophysical Properties Database of Materials for Light Water Reactors and Heavy Water Reactors, IAEA TECDOC Series (International Atomic Energy Agency, 2006).
- [21] C. Sevik, T. Çağ in, Phys. Rev. B 80 (2009) 014108.
- [22] V. Kanchana, G. Vaitheeswaran, A. Svane, A. Delin, J. Phys. Condens. Matter 18 (2006) 9615.
- [23] I. Shein, K. Shein, A. Ivanovskii, J. Nucl. Mater. 361 (2007) 69.
- [24] B.-T. Wang, H. Shi, W.-D. Li, P. Zhang, J. Nucl. Mater. 399 (2010) 181.
- [25] B. J. C. Int. J. Quant. Chem. 109 (2009) 3564. <https://onlinelibrary.wiley.com/doi/pdf/10.1002/qua.22376>.
- [26] A. Boudjemline, L. Louail, M.M. Islam, B. Diawara, Comput. Mater. Sci. 50 (2011) 2280.
- [27] G. Kresse, J. Furthmüller, Phys. Rev. B 54 (1996) 11169.
- [28] G. Kresse, J. Furthmüller, Comput. Mater. Sci. 6 (1996) 15.
- [29] W. Li, J. Carrete, N.A. Katcho, N. Mingo, Comput. Phys. Commun. 185 (2014) 1747.
- [30] A. Togo, F. Oba, I. Tanaka, Phys. Rev. B 78 (2008) 134106.
- [31] J.P. Perdew, K. Burke, M. Ernzerhof, Phys. Rev. Lett. 77 (1996) 3865.
- [32] G. Kresse, D. Joubert, Phys. Rev. B 59 (1999) 1758.
- [33] P. Zhang, B.-T. Wang, X.-G. Zhao, Phys. Rev. B 82 (2010) 144110.
- [34] J.S. Olsen, L. Gerward, V. Kanchana, G. Vaitheeswaran, J. Alloy. Comp. 381 (2004) 37.
- [35] M. Idiri, T. Le Bihan, S. Heathman, J. Rebizant, Phys. Rev. B 70 (2004), 014113.
- [36] Y. Zhao, Z. Dai, C. Zhang, C. Lian, S. Zeng, G. Li, S. Meng, J. Ni, Phys. Rev. B 95 (2017), 014307.
- [37] C. Ronchi, M. Sheindlin, M. Musella, G.J. Hyland, J. Appl. Phys. 85 (1999) 776. <https://doi.org/10.1063/1.369159>.
- [38] Y.N. Devyatko, V.V. Novikov, V.I. Kuznetsov, O.V. Khomyakov, D.A. Chulkin, IOP Conf. Ser. Mater. Sci. Eng. 130 (2016) 012061.
- [39] J.-J. Ma, J.-G. Du, M.-J. Wan, G. Jiang, J. Alloy. Comp. 627 (2015) 476.
- [40] M. W. D. Cooper, S. T. Murphy, P. C. M. Fossati, M. J. D. Rushton, and R. W. Grimes, 470 (2014), 10.1098/rspa.2014.0427.
- [41] X. Yang, Z. Dai, Y. Zhao, S. Meng, Comput. Mater. Sci. 147 (2018) 132.
- [42] W. Li, J. Carrete, N. Mingo, Appl. Phys. Lett. 103 (2013) 253103. <https://doi.org/10.1063/1.4850995>.
- [43] X. Yang, Y. Zhao, Z. Dai, M. Zulfiqar, J. Zhu, J. Ni, Phys. Lett. 381 (2017) 3514.
- [44] B. Peng, H. Zhang, H. Shao, Y. Xu, X. Zhang, H. Zhu, Sci. Rep. 6 (2016) 20225.
- [45] Y. Zhao, Z. Dai, C. Lian, S. Meng, RSC Adv. 7 (2017) 25803.
- [46] J. Ziman, Sci. Am. 217 (1967) 180, a division of Nature America, Inc.
- [47] W. Li, N. Mingo, Phys. Rev. B 89 (2014) 184304.
- [48] W. Li, N. Mingo, Phys. Rev. B 91 (2015) 144304.
- [49] L. Lindsay, D.A. Broido, J. Phys. Condens. Matter 20 (2008) 165209.
- [50] T. Tadano, Y. Gohda, S. Tsuneyuki, Phys. Rev. Lett. 114 (2015) 095501.
- [51] F. Giorgia, C. Andrea, P. Lorenzo, L. Michele, M. Nicola, M. Francesco, Nano Letters (Print) 14 (2014) 6109, eng.
- [52] B. Peng, H. Zhang, H. Shao, Y. Xu, X. Zhang, H. Zhu, Ann. Phys. 528 (2016) 504.